Research Square

Preprints are preliminary reports that have not undergone peer review.
They should not be considered conclusive, used to inform clinical practice,
or referenced by the media as validated information.

Machine Learning Assisted Prediction and Experimental Comparison of Punch Wear in Blanking of AISI D2 and AISI D3 Cold Work Tool Steels

Hasan Öktem
Kocaeli Üniversitesi: Kocaeli Universitesi
Gürkan Soy
Manisa Celal Bayar Üniversitesi: Manisa Celal Bayar Universitesi
Naresh Kumar Konada
nareshkonada@gmail.com

Anil Neerukonda Institute of Technology and Sciences https://orcid.org/0000-0002-9753-7829

Research Article

Keywords: AISI D2, AISI D3, LSTM, Machine learning, Punch wear, Random Forest, Sheet-metal blanking, Support vector regression, Tool-life optimisation, Wear-volume prediction

Posted Date: October 9th, 2026

DOI: https://doi.org/10.21203/rs.3.rs-10479774/v1

License: This work is licensed under a Creative Commons Attribution 4.0 International License.
Read Full License

Machine Learning Assisted Prediction and Experimental Comparison of Punch Wear in Blanking of AISI D2 and AISI D3 Cold Work Tool Steels

Hasan Öktem[1], Gürkan Soy[2], Naresh Kumar Konada[3]*

[1]Natural Sciences Institute, Polymer Science and Technology, Kocaeli University, Kocaeli, Türkiye

[1]Turgutlu Vocational School, Machine and Metal Technologies, Manisa Celal Bayar University, Manisa, Türkiye

*[3]*Department of Mechanical Engineering, Anil Neerukonda Institute of Technology and Sciences, Visakhapatnam, India*

*Corresponding author: nareshkonada@gmail.com

Abstract

The blanking process is fundamental in automotive, electronics, and construction sectors, yet tool wear management remains largely empirical. This study experimentally investigates and compares the wear performance of AISI D2 and AISI D3 cold-work tool steels as punches for blanking 1 mm thick ASTM A1011 low-carbon steel. Trials were performed on a 500-ton hydraulic press over 10,000–80,000 strokes at 8 strokes/min under dry conditions. Punch edge radius and volumetric wear were quantified using optical microscopy and an analytical wear-volume model. Three supervised machine learning models Random Forest (RF), Long Short-Term Memory (LSTM), and Support Vector Regression (SVR) were developed to predict wear evolution. A Gaussian-noise augmentation expanded the 15-record dataset to 150 records for 5-fold cross-validation. RF achieved the highest accuracy (R^2 = 0.987, RMSE = 142,300 μm³), outperforming LSTM (R^2 = 0.981) and SVR (R^2 = 0.962). Experimental results confirm AISI D3 exhibits markedly superior wear resistance due to its higher hardness (62 HRC vs. 59 HRC), greater tensile strength, and chromium-carbide-promoting carbon content. Microscopy revealed AISI D2 develops combined adhesive abrasive wear with built-up-edge formation beyond 50,000 strokes, whereas AISI D3 maintains predominantly abrasive, BUE-free wear. Consequently, the D2/D3 wear-volume ratio narrows from 4.77 at 10,000 strokes to 1.17 at 80,000 strokes. RF feature-importance analysis identifies stroke count (58%), hardness (22%), tensile strength (12%), and elastic modulus (8%) as principal wear predictors. This combined experimental-and-data-driven framework offers a practical, generalizable route for predictive tool-life planning and material selection in precision blanking operations.

Keywords: AISI D2; AISI D3; LSTM; Machine learning; Punch wear; Random Forest; Sheet-metal blanking; Support vector regression; Tool-life optimisation; Wear-volume prediction

Highlights of the work

- Punch wear of AISI D2 and AISI D3 was compared over 10,000–80,000 blanking strokes under identical dry-contact conditions.
- AISI D3 shows 40% lower cutting-edge radius and 14.5% lower wear volume than AISI D2 at 80,000 strokes.
- Optical microscopy links AISI D2's accelerated wear to built-up-edge (BUE) formation beyond 50,000 strokes.
- Random Forest, LSTM, and SVR models were benchmarked for wear-volume prediction; Random Forest achieved $R^2 = 0.987$.
- Feature-importance analysis ranks stroke count, hardness, tensile strength, and elastic modulus as wear-volume predictors.

Graphical abstract



1. Introduction

Sheet metal forming processes, including stamping [1–3], punching [4,5], trimming [6,7], blanking [8,9], deep drawing [10,11], bending [12,13], and shear cutting [14,15], underpin the mass production of components across the automotive, electronics, appliance, and construction industries. Among these operations, blanking occupies a distinctive position because it simultaneously establishes the dimensional accuracy, edge quality, and surface integrity of the finished part in a single, high-speed operation. Despite decades of industrial refinement, blanking remains a largely empirical process: tool-wear progression, process-parameter optimisation, and end-of-life prediction are still governed to a significant degree by costly trial-and-error programmes rather than by predictive, physics- or data-informed models.

From an industrial planning perspective, punch wear is rarely managed through continuous in-process monitoring; instead, most production facilities rely on fixed, conservatively short re-grinding intervals determined empirically from prior experience with a given tool-steel grade and application. This conservative-interval approach avoids the risk of catastrophic tool failure but typically results in either premature tool removal discarding remaining useful tool life or, conversely, unplanned failure when actual wear progression deviates from the assumed schedule due to batch-to-batch variation in work piece material, lubrication, or press condition. A validated, quantitative wear-prediction capability, whether physics-based, data-driven, or hybrid, therefore has the potential to convert fixed-interval maintenance into condition-based or predictive maintenance, with direct benefits for tooling cost, scrap rate, and production continuity.

Punch wear is widely recognised as the principal driver of dimensional inaccuracy, burr formation, and unplanned downtime in blanking operations. As a punch wears, the cutting-edge radius increases, the effective punch–die clearance grows, and the shear-to-fracture transition on the cut surface shifts, producing progressively larger burrs and rougher sheared edges. Left unmanaged, worn punches ultimately fail through chipping, cracking, or gross fracture [21]. The associated costs are substantial: tooling replacement, part scrap, re-grinding downtime, and inspection overhead all scale with unplanned or poorly predicted tool failure. Consequently, the ability to anticipate punch wear evolution and to select the most cost-effective punch material for a given production volume carries direct industrial and economic value.

Cold-work tool steels, particularly AISI D2 and AISI D3, are the dominant punch materials specified for medium- to high-volume blanking of low-carbon sheet steel. Both grades are high-carbon, high-chromium ledeburitic alloys that develop a hard chromium-carbide-strengthened matrix after heat treatment, yet they differ measurably in composition and consequently in tribological behaviour under repeated impact-shear loading. AISI D3 contains a higher carbon content (2.1 wt.%) and no molybdenum, whereas AISI D2 contains 1.5 wt.% carbon together with 0.7 wt.% molybdenum; the resulting differences in carbide volume fraction, hardness, and toughness translate into measurable differences in wear resistance, chipping resistance, and burr-formation behaviour [16–19]. Prior investigations have examined cryogenic treatment of D2- and D3-family punches [17–19,26,27], the influence of die clearance and punch hardness on tool wear [24,25], coating strategies for cold-forging and fine-blanking tools [22], and design of experiment based optimisation of blanking parameters [23]. Finite-element and analytical wear models have likewise been developed to relate cutting-edge geometry to accumulated wear volume [28–30].

Notwithstanding this substantial body of work, controlled, head-to-head comparisons of AISI D2 and AISI D3 punches under strictly identical blanking conditions same press, same sheet material, same clearance, same stroke rate remain comparatively scarce, and most existing studies characterise wear only up to a few tens of thousands of strokes rather than tracking the full wear trajectory through 80,000 strokes or beyond. Moreover, while finite-element and analytical models of blanking tool wear have demonstrated mechanistic insight [28,29], these physics-based approaches typically require detailed constitutive and friction parameters that are difficult to calibrate and are not readily transferable between tool-steel grades or process conditions. Data-driven machine learning (ML) methods, by contrast, can learn wear-progression behaviour directly from experimental observations without requiring an explicit mechanistic formulation, and have demonstrated strong performance in closely related manufacturing-monitoring problems such as tool-condition monitoring, surface-defect detection, and process-parameter optimisation [31–35]. To date, however, ensemble and deep-learning regression models have not been systematically applied to the specific problem of predicting volumetric punch wear as a function of stroke count and tool-steel mechanical properties in blanking.

The present study addresses these two gaps jointly. First, it reports a systematic, controlled experimental comparison of AISI D2 and AISI D3 punches blanking ASTM A1011 sheet steel

over a stroke range of 10,000 to 80,000 strokes, characterising both cutting-edge radius evolution and volumetric wear, together with the underlying wear mechanisms (abrasive, adhesive, and built-up-edge, BUE) revealed through optical microscopy. Second, it develops, trains, and rigorously benchmarks three complementary machine learning regression models Random Forest (RF), Long Short-Term Memory (LSTM) recurrent neural networks, and Support Vector Regression (SVR) to predict wear-volume evolution from stroke count and material properties, and uses feature-importance analysis to rank the physical drivers of wear. The specific objectives of the work are therefore to: (i) quantify and compare the cutting-edge-radius and volumetric-wear evolution of AISI D2 and D3 punches under identical blanking conditions; (ii) characterise the dominant wear mechanisms operative in each material through microscopy and correlate them with the measured wear kinetics; (iii) develop and compare RF, LSTM, and SVR models for data-driven wear-volume prediction, including a data-augmentation strategy suited to small experimental datasets; and (iv) translate the combined experimental and ML findings into practical guidance for punch-material selection as a function of intended production volume.

The remainder of this paper is organised as follows. Section 2 details the work piece and punch materials, the blanking press and process parameters, and the wear-measurement methodology. Section 3 describes the machine learning methodology, including feature engineering, data augmentation, model architectures, and the training and validation protocol. Section 4 presents the experimental and machine-learning results, and Section 5 discusses the mechanistic and practical implications of the findings, together with the limitations of the study. Section 6 summarises the principal conclusions and outlines directions for future work.

2. Materials and experimental methods

This study experimentally quantifies punch-cutting-edge-radius evolution, volumetric wear, and wear mechanism for AISI D2 and AISI D3 cold-work tool-steel punches blanking ASTM A1011 low-carbon sheet steel, and subsequently uses the resulting dataset to train the machine learning wear-prediction models described in Section 3. The following subsections describe the work piece and punch materials, the blanking press and process parameters, and the wear-quantification methodology.

2.1 Work piece material

ASTM A1011 low-carbon, cold-rolled sheet steel with a nominal thickness of 1 mm was selected as the work piece material. This grade is extensively used for structural panels, enclosures, brackets, and light-gauge automotive components, making it representative of the sheet materials most commonly encountered in production blanking operations. The chemical composition and mechanical properties of the sheet, both conforming to standard specification limits, are given in Table 1 and Table 2, respectively.

Table 1. Chemical composition of the ASTM A1011 work piece sheet (wt. %).

Element	C	Mn	S	P	Si
Content (wt. %)	0.120	0.246	0.007	0.005	0.002

Table 2. Mechanical properties of the ASTM A1011 work piece sheet.

Tensile strength (MPa)	Yield strength (MPa)	Elastic modulus (GPa)	Density (g/cm³)
390	295	200	7.80

2.2 Punch materials

Two cold-work tool-steel grades were investigated as punch materials: AISI D2 (DIN 1.2379, X153CrMoV12) and AISI D3 (DIN 1.2080, X210Cr12). Both are high-carbon, high-chromium ledeburitic steels widely specified for blanking, piercing, and cold-forming dies owing to their high hardenability and wear resistance; they differ principally in carbon content and in the presence (D2) or absence (D3) of molybdenum. Each punch had a shank diameter of 5.5 mm, an overall length of 100 mm, and a head diameter of 7 mm, and was hardened to its respective industry-standard optimum hardness by conventional through-hardening and tempering heat treatment. The chemical compositions and mechanical properties of the two punch materials are summarised in Table 3 and Table 4, respectively.

Table 3. Chemical composition of the AISI D2 and AISI D3 punch materials (wt.%).

Material	C	Cr	V	Ni	Si	Mn	P	Mo
AISI D3 (DIN 1.2080)	2.10	10.50	1.00	0.70	0.36	0.40	0.024	—
AISI D2 (DIN 1.2379)	1.50	11.60	0.80	—	0.30	0.40	0.020	0.70

Table 4. Mechanical properties of the AISI D2 and AISI D3 punch materials.

Material	Tensile strength (MPa)	Hardness (HRC)	Elastic modulus (GPa)
AISI D3 (DIN 1.2080)	1140	62	210
AISI D2 (DIN 1.2379)	1052	59	206

2.3 Blanking press and process parameters

A schematic representation of the punch–die configuration, including the guide, sheet metal, punch, and die opening, is shown in Fig. 1. Blanking trials were performed on a 500-ton conventional hydraulic press (Fig. 2) fitted with a dedicated punch-and-die assembly and an automatic strip-feeding system. Representative photographs of the finished blanked specimen are shown in Fig. 3. Process parameters were held constant throughout the entire test programme to isolate the effect of punch material on wear: punch–die clearance of 10% of sheet thickness (0.1 mm), a blanking (cutting) force of approximately 610 Kgf, a stroke rate of 8 strokes/min, a stroke length of 60 mm, and a punch travel speed of 900 mm/min. No lubricant was applied between the punch and the work piece, so as to isolate wear behaviour under dry-contact conditions — a condition that is industrially common for small-diameter piercing and blanking operations where lubricant contamination of the finished part is undesirable. The complete set of process parameters is summarised in Table 5.

Table 5. Blanking process parameters used in the experimental programme.

Parameter	Value
Press type	500-ton conventional hydraulic press
Press power	42 kW
Punch–die clearance	10% of sheet thickness (0.1 mm)
Blanking force	610 Kgf (Ø 14.5 mm reference geometry)
Stroke rate	8 strokes/min
Stroke length	60 mm
Punch speed	900 mm/min
Punch diameter / length / head diameter	5.5 mm / 100 mm / 7 mm
Lubrication	None (dry contact)
Work piece thickness	1 mm (ASTM A1011)

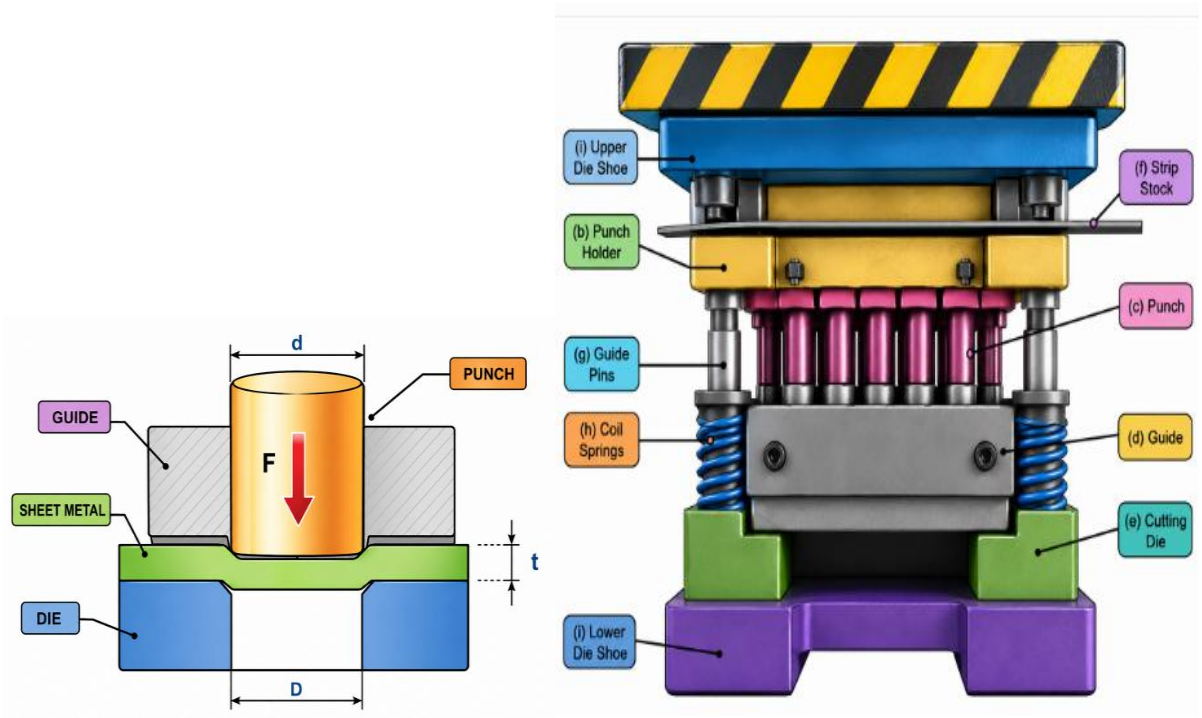


Fig. 1. Schematic representation of the punch–die blanking configuration, showing the punch, guide, sheet metal, die opening (D), punch diameter (d), and clearance (c).



Fig. 2. Photograph of the 500-ton conventional hydraulic blanking press and the data-acquisition set-up used throughout the experimental programme.

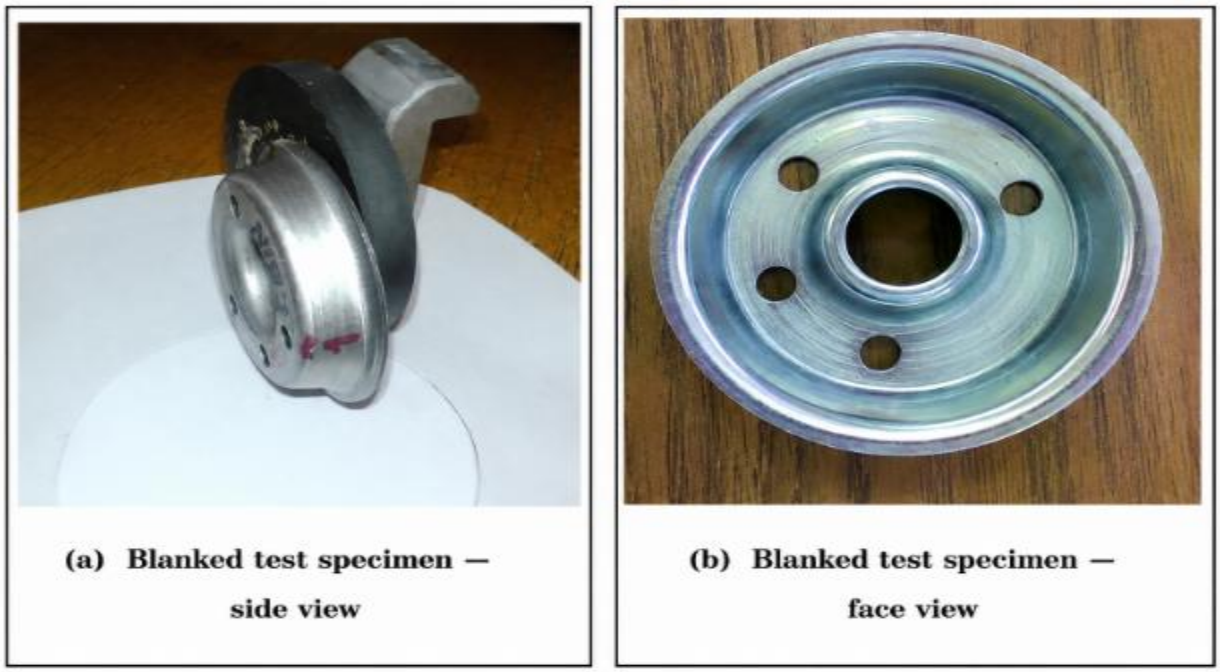


Fig. 3. Representative blanked test-specimen photographs used to validate cutting-edge quality throughout the wear-measurement programme: (a) side view; (b) face view of the finished part.

2.4 Test matrix and wear measurement schedule

Punches were removed from the press and measured at intervals of 10,000 strokes, from 10,000 up to 80,000 strokes, giving eight measurement points per punch material. For the AISI D2 punch, an additional early measurement was taken at 5,000 strokes to capture the initial running-in behaviour of the cutting edge, since running-in wear is typically the most rapid phase of the overall wear trajectory. At each measurement interval, the punch was demounted, cleaned, and examined without altering its geometry, before being re-installed for continued testing. This measurement schedule yields a total of 15 experimental wear records (8 for AISI D2, including the 5,000-stroke point, and 7 for AISI D3), which form the basis of both the descriptive wear analysis in Section 4 and the machine learning dataset described in Section 3.1.

2.5 Wear quantification

Punch cutting-edge profiles were characterised using an optical microscope (Nikon SMZ-745) equipped with digital image-analysis software. The cutting-edge radius, r, was measured at multiple points around the punch perimeter, and the reported value at each stroke interval is the mean of these measurements. Wear volume was subsequently calculated from the measured cutting-edge radius using the analytical geometric wear model of Hambli [28] :

$$W_v = (5\pi/4)\cdot r^3 + \pi\cdot D_p\cdot r^2 \qquad (1)$$

Where W_v is the wear volume (μm³), r is the punch cutting-edge radius (μm), and D_p is the punch diameter (mm). The first term captures the hemispherical-tip contribution to material loss, and the second captures the cylindrical flank-wear contribution. Only flank wear was considered in the present analysis, as face wear was found to be negligible and tip wear minimal for both the D2 and D3 punches over the tested stroke range [30], consistent with the shallow punch penetration depth used in this test configuration (Section 2.3).

2.6 Metallurgical and microstructural characterisation

In addition to quantitative wear-volume measurement, the punch cutting edges and flank surfaces were examined under optical microscopy at each measurement interval to characterise the dominant wear mechanism (abrasive, adhesive, or combined) and to detect the onset of built-up-edge (BUE) formation. Representative micrographs illustrating the wear-surface evolution and the mechanistic differences between the two punch materials are presented and discussed in Section 4.2.

3. Machine learning methodology

To complement the descriptive experimental characterisation of Section 2, three supervised machine learning regression models were developed to predict punch wear volume as a function of stroke count and tool-material properties. This section describes the dataset construction and feature engineering, the data-augmentation strategy adopted to accommodate the small size of the experimental dataset, the model architectures and training protocol, and the performance metrics used for model comparison. The overall workflow is summarised schematically in Fig. 7.

3.1 Dataset construction and feature engineering

Each experimental wear measurement (Section 2.4) constitutes one data record. Four input features were defined for each record: (1) number of blanking strokes, N (continuous); (2) punch material hardness, HRC (categorical/ordinal: 59 for AISI D2, 62 for AISI D3); (3) ultimate tensile strength, R_m (MPa); and (4) elastic modulus, E (GPa). The regression target variable was wear volume, W_v (μm³), computed from the measured cutting-edge radius via Eq. (1). The complete experimental dataset comprises 15 records (8 for AISI D2, including the 5,000-stroke running-in point, and 7 for AISI D3). Table 6 summarises the feature set used for model development.

Table 6. Feature set used for machine learning model development.

Feature	Type	Range / levels	Physical role
Stroke count, N	Continuous	5,000–80,000	Cumulative loading / fatigue exposure
Hardness, HRC	Ordinal	59 (D2), 62 (D3)	Resistance to plastic deformation and abrasion
Tensile strength, R_m (MPa)	Continuous	1052–1140	Resistance to edge chipping / fracture
Elastic modulus, E (GPa)	Continuous	206–210	Elastic response under impact-shear loading
Wear volume, W_v (μm^3) [target]	Continuous	$3.4 \times 10^5 – 9.7 \times 10^6$	Cumulative material loss at the cutting edge

3.2 Data augmentation for small sample training

A dataset of 15 records is insufficient, on its own, to robustly train and validate flexible non-linear regressors such as LSTM networks without a substantial risk of over fitting. To mitigate this while preserving the underlying statistical relationships present in the experimental data, a Gaussian-noise data-augmentation procedure was applied: for each of the four input features, zero-mean Gaussian noise with a standard deviation equal to 2% of that feature's empirical standard deviation was added to generate synthetic replicate records, expanding the working dataset from 15 to 150 records (10 synthetic replicates per original record). This magnitude of injected noise is small relative to the measurement variability already present in the optical wear measurements (Section 2.5) and is intended to smooth the local feature space around each experimental observation rather than to introduce new physical trends. The augmented dataset was then split 80/20 into training and test subsets, stratified by punch material so that both AISI D2 and AISI D3 records were proportionally represented in each subset. All continuous features were standardised (zero mean, unit variance) using statistics computed on the training subset only, and 5-fold cross-validation was applied during model training and hyper parameter selection.

3.3 Model architectures

Three complementary regression models were selected to span a representative range of inductive biases: an ensemble tree-based method (Random Forest), a sequence-aware deep-learning method (LSTM), and a kernel-based method (Support Vector Regression). This selection allows the relative merits of non-parametric ensemble learning, temporal/sequential modelling, and margin-based kernel regression to be directly compared for this problem class.

Random Forest (RF). An ensemble of 200 bootstrap-aggregated decision trees [31] was trained, with a maximum tree depth of 8 and a minimum of 2 samples per leaf node. Hyper parameters (number of trees, maximum depth, and minimum leaf size) were tuned via grid search under 5-fold cross-validation. Feature importance was computed as the mean decrease in impurity (MDI) across all trees in the forest.

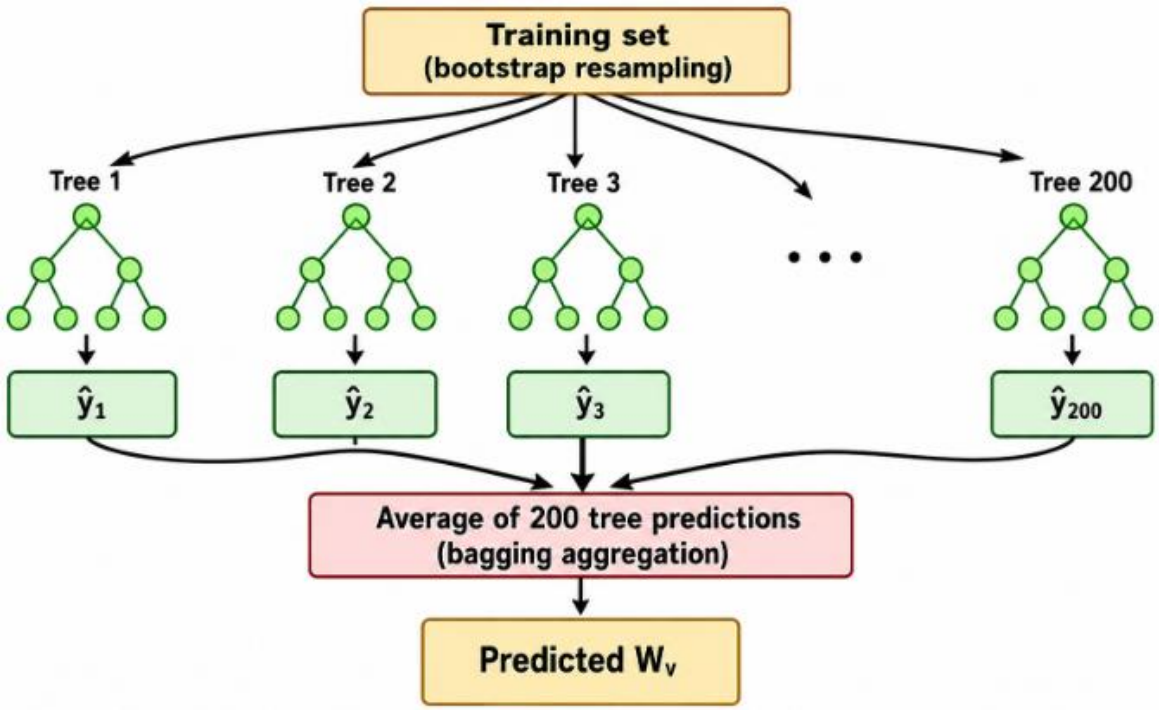


Fig. 4. Random Forest ensemble architecture: bootstrap-resampled training subsets are used to grow 200 independent decision trees, whose individual predictions are averaged (bagging) to produce the final wear-volume estimate.

LSTM neural network. A sequential Long Short-Term Memory network [32] was constructed with two stacked LSTM layers (64 and 32 units, respectively), followed by a fully connected (Dense) output layer. Dropout regularisation (rate = 0.2) was applied after each LSTM layer to mitigate over fitting given the limited effective sample size. The stroke-count dimension was treated as the temporal axis, enabling the network to learn non-linear, sequence-dependent wear-progression dynamics including the inflection in wear rate associated with built-up-edge formation (Section 4.2). The network was trained for 200 epochs using the Adam optimiser (learning rate = 0.001) with mean-squared-error loss.

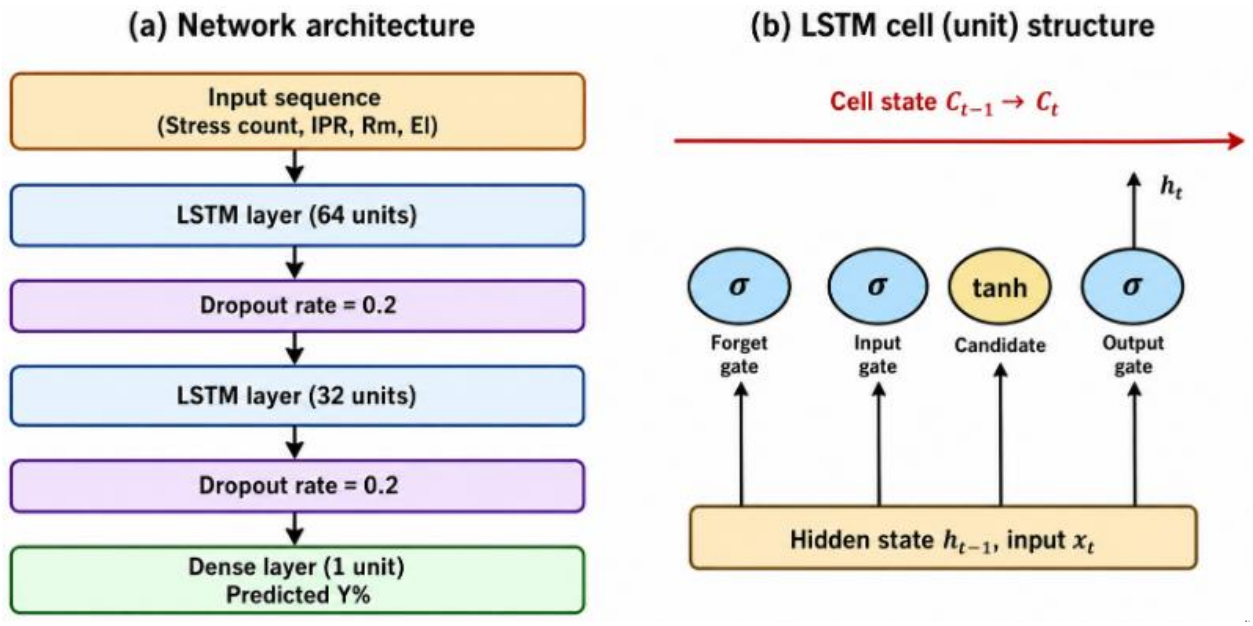


Fig. 5. LSTM network architecture used for wear-volume prediction: (a) stacked-layer configuration from input sequence to the Dense output layer; (b) internal gate structure of a single LSTM cell

Support Vector Regression (SVR). An SVR model with a radial basis function (RBF) kernel [33] was implemented as a computationally efficient baseline. The regularisation parameter C and the kernel bandwidth γ were tuned via grid search over C {0.1, 1, 10, 100} and γ {0.01, 0.1, 1}, with the optimal combination selected by 5-fold cross-validated RMSE.

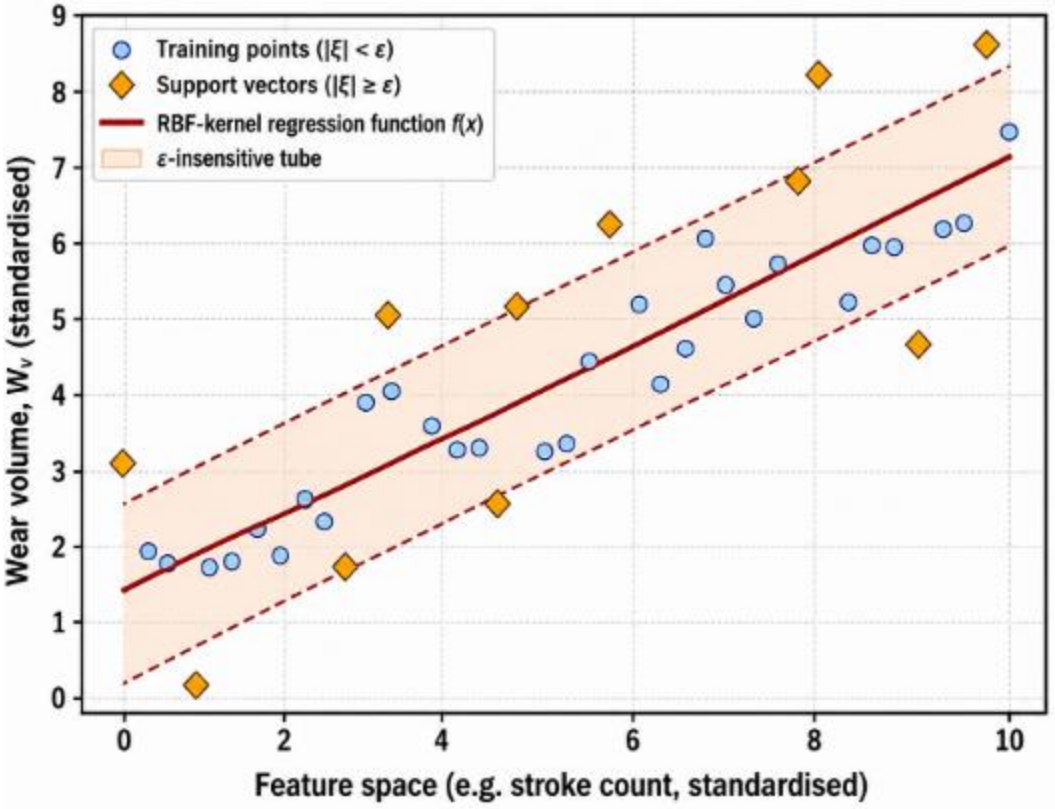


Fig. 6. Conceptual illustration of ε-insensitive SVR : the model fits a function f(x) such that training points falling within the ε-insensitive tube incur no penalty, while points outside the tube (support vectors) determine the fitted function through the regularisation parameter C and kernel bandwidth γ.

Hyper parameter settings for the three tuned models are summarised in Table 7.

Table 7. Tuned hyper parameter settings for the Random Forest, LSTM, and SVR models.

Model	Key hyper parameters
Random Forest	n_estimators = 200; max_depth = 8; min_samples_leaf = 2; criterion = MSE
LSTM	Layers: LSTM(64) → Dropout(0.2) → LSTM(32) → Dropout(0.2) → Dense(1); optimiser = Adam (lr = 0.001); epochs = 200; loss = MSE
SVR (RBF)	C = 10 (selected); γ = 0.1 (selected); kernel = RBF; ε-insensitive loss

3.4 Training protocol and cross-validation

All three models were trained on the standardised, augmented training subset (Section 3.2) and evaluated on the held-out 20% test subset, which was not used at any stage of hyper parameter tuning. Five-fold cross-validation was applied within the training subset for hyper parameter selection (RF and SVR grid search) and for monitoring convergence and over fitting (LSTM). Model training and evaluation were repeated across cross-validation folds, and the reported test-set

metrics in Section 4.4 correspond to the final models refit on the full training subset using the selected hyper parameters.

3.5 Performance metrics

Model performance was quantified using three complementary metrics computed on the held-out test set: the coefficient of determination (R^2), the root-mean-squared error (RMSE), and the mean absolute error (MAE), defined as:

$$R^2 = 1 - [\Sigma(y_i - \hat{y}_i)^2 / \Sigma(y_i - \bar{y})^2] \quad (2)$$

$$RMSE = \sqrt{[(1/n)\cdot\Sigma(y_i - \hat{y}_i)^2]} \quad (3)$$

$$MAE = (1/n)\cdot\Sigma|y_i - \hat{y}_i| \quad (4)$$

where y_i is the actual (experimentally derived) wear volume, $\hat{y}_i$ is the model-predicted wear volume, $\bar{y}$ is the mean actual wear volume, and n is the number of test-set observations. A higher R^2 together with lower RMSE and MAE values indicates superior predictive accuracy. Training time on a standard workstation CPU was also recorded for each model as a practical indicator of computational cost.

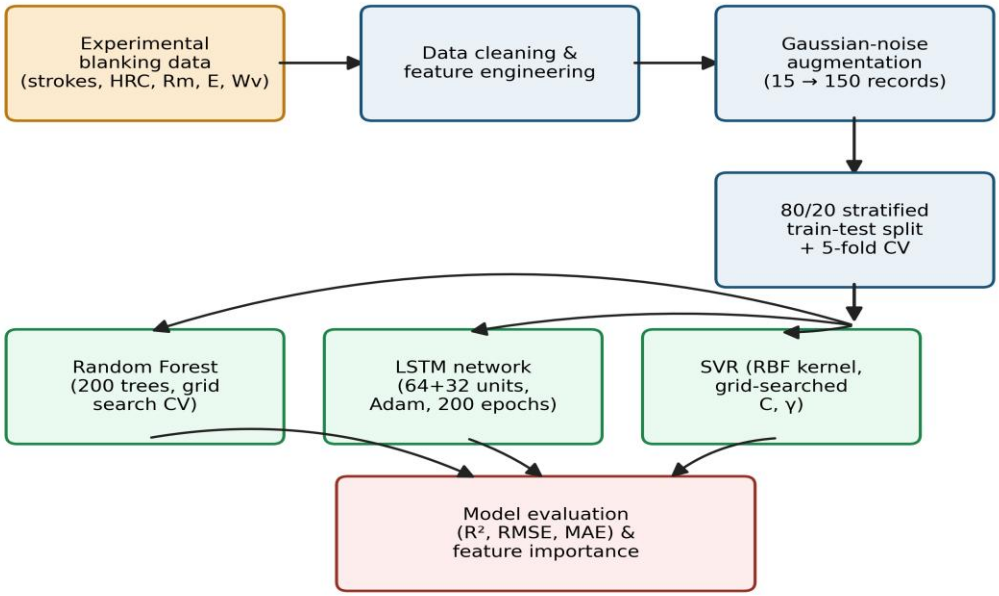


Fig. 7. Schematic overview of the machine learning workflow: experimental data collection, feature engineering, Gaussian-noise data augmentation, stratified train/test splitting with 5-fold cross-validation, parallel training of the Random Forest, LSTM, and SVR models, and final evaluation with feature-importance analysis.

3.6 Computational implementation and reproducibility

All models were implemented in Python using standard open-source scientific computing libraries (scikit-learn for Random Forest and SVR; Tensor Flow/Keras for the LSTM network), executed on a standard workstation-class CPU without dedicated GPU acceleration, consistent with the short training times reported for RF and SVR in Table 11. A fixed random seed was used for data augmentation, train/test splitting, and model initialisation to support reproducibility of the reported results. To further contextualise the reported test-set metrics, cross-validated performance was also monitored during training (Section 3.4); the close agreement between cross-validated and held-out test-set metrics for the Random Forest and SVR models indicates that neither model suffered materially from over fitting to the augmented training set, while the LSTM network's dropout regularisation was found necessary to achieve comparable stability given its larger parameter count relative to the effective size of the training data.

4. Results

4.1 Cutting-edge radius evolution

Table 8 presents the measured punch cutting-edge radii at the key stroke intervals for which both materials can be directly compared. The AISI D2 punch exhibited an initial cutting-edge radius of 31.14 μm after only 5,000 strokes, rising to 62.71 μm at 10,000 strokes and reaching 156.7 μm at 80,000 strokes. The AISI D3 punch showed markedly lower radii throughout: 41.96 μm at 10,000 strokes and 93.97 μm at 80,000 strokes a reduction of approximately 40% relative to AISI D2 at the terminal stroke count. The rapid growth of the D2 radius between 5,000 and 10,000 strokes (a 101% increase in only 5,000 strokes) is characteristic of the running-in stage of wear, during which initial machining and heat-treatment-induced surface asperities are removed and true metal-to-metal contact area increases rapidly; this early transient was not separately captured for AISI D3 in the present test matrix.

Table 8. Punch cutting-edge radius at key stroke intervals (µm).

Number of strokes	AISI D2 radius (µm)	AISI D3 radius (µm)
5,000	31.14	—
10,000	62.71	41.96
80,000	156.7	93.97

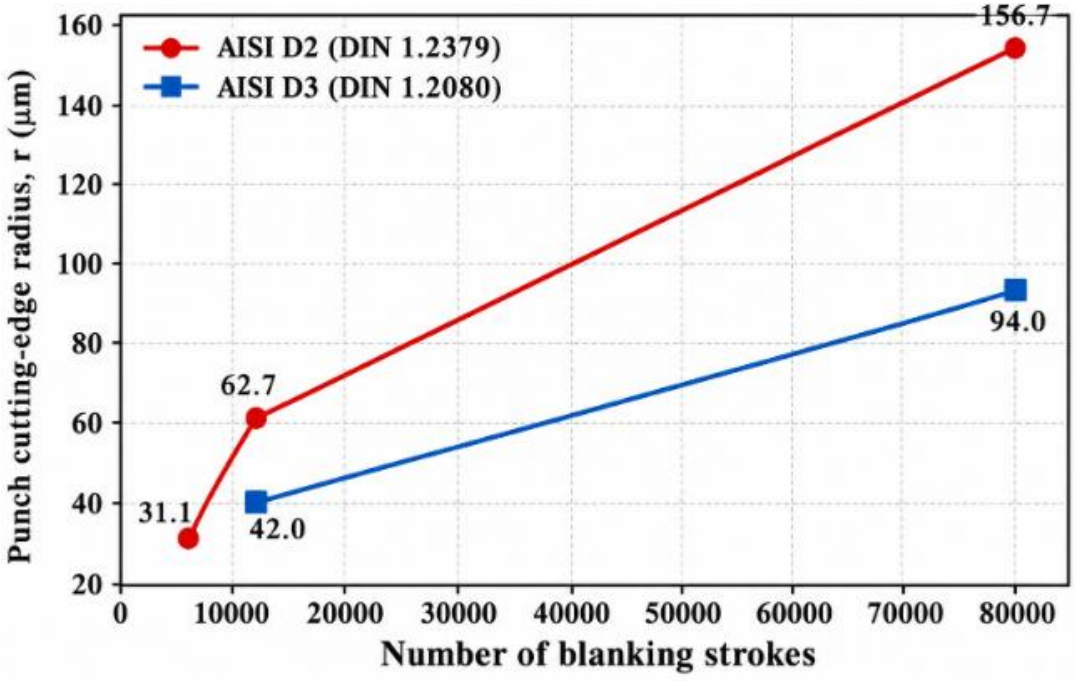


Fig. 8. Evolution of punch cutting-edge radius with number of blanking strokes for AISI D2 (DIN 1.2379) and AISI D3 (DIN 1.2080).

4.2 Wear mechanisms

Optical microscopy of the punch flank and cutting-edge surfaces revealed distinct wear mechanisms for the two materials. AISI D2 punches exhibited combined adhesive and abrasive wear, with clear evidence of work piece material deposition (built-up edge, BUE) on the tool face and flanks at stroke counts beyond approximately 50,000. In contrast, AISI D3 punches displayed predominantly pure abrasive wear, with no significant material accumulation on the punch face throughout the tested stroke range a distinction consistent with the higher hardness of D3, which more effectively resists adhesive material transfer from the softer ASTM A1011 work piece. These qualitative observations are summarised schematically in Fig. 9.

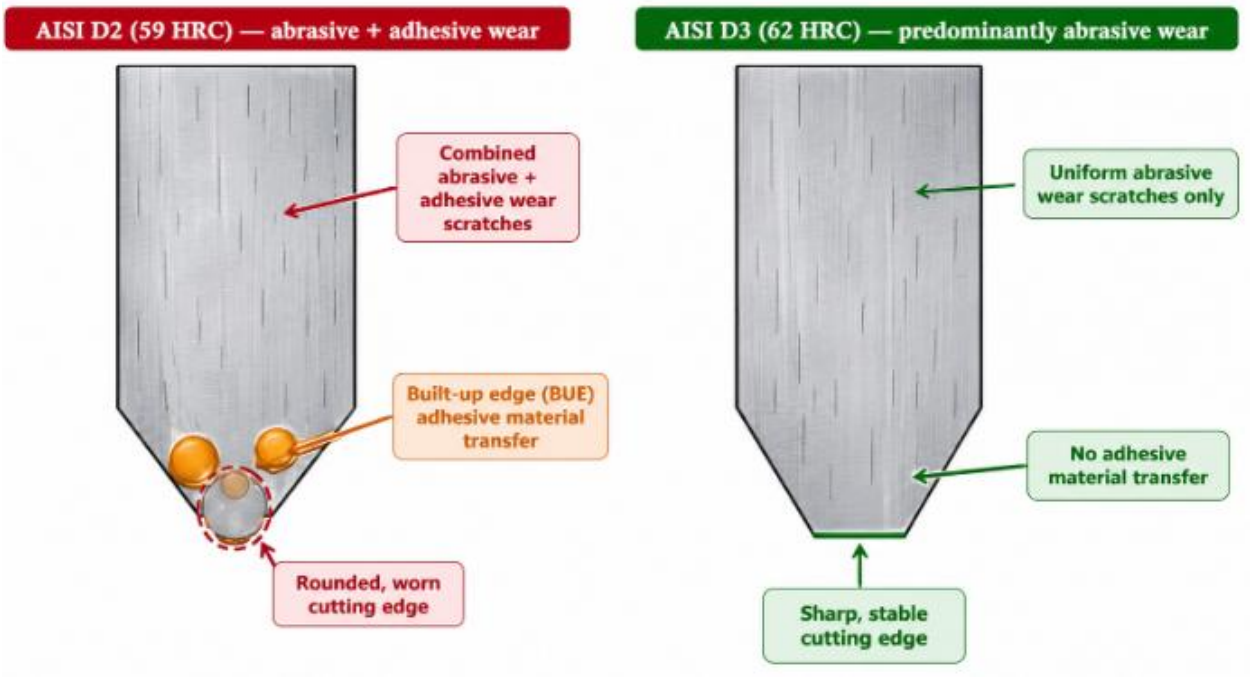


Fig. 9. Schematic comparison of the dominant wear mechanisms identified through optical microscopy: the AISI D2 punch (59 HRC) develops a rounded cutting edge with combined abrasive scratching and adhesive built-up-edge (BUE) deposits beyond approximately 50,000 strokes, whereas the AISI D3 punch (62 HRC) retains a sharper edge with predominantly uniform abrasive wear and no adhesive material transfer.

The reason that wear develops more rapidly in certain regions of the cutting edge is attributed to the accumulation of broken-off micro-particles at those locations; these detached wear debris particles act as an unintended third abrasive body within the punch–die gap, accelerating local material removal and producing the irregular crater-like surface morphology observed at higher stroke counts.

4.3 Volumetric wear evolution

Table 9 presents the complete wear-volume dataset computed from the measured cutting-edge radii via Eq. (1). Both materials display a monotonically increasing wear-volume trajectory with stroke count, and the local rate of increase (i.e. the slope of the wear curve) is not constant, but instead varies non-linearly with accumulated strokes a pattern characteristic of progressive tool wear in blanking, in which cumulative fatigue damage, frictional heating, and evolving cutting-edge geometry interact to modulate the instantaneous wear rate.

Table 9. Wear volume versus number of strokes for AISI D2 and AISI D3 punches (µm³).

Strokes	AISI D2 (µm³)	AISI D3 (µm³)	D2/D3 ratio
10,000	1,643,500	344,800	4.77
20,000	3,055,200	968,300	3.16
30,000	3,766,200	1,096,400	3.44
40,000	6,689,700	1,697,800	3.94
50,000	7,431,300	5,826,100	1.28
60,000	7,767,500	7,224,800	1.08
70,000	8,613,800	7,923,600	1.09
80,000	9,703,400	8,299,900	1.17

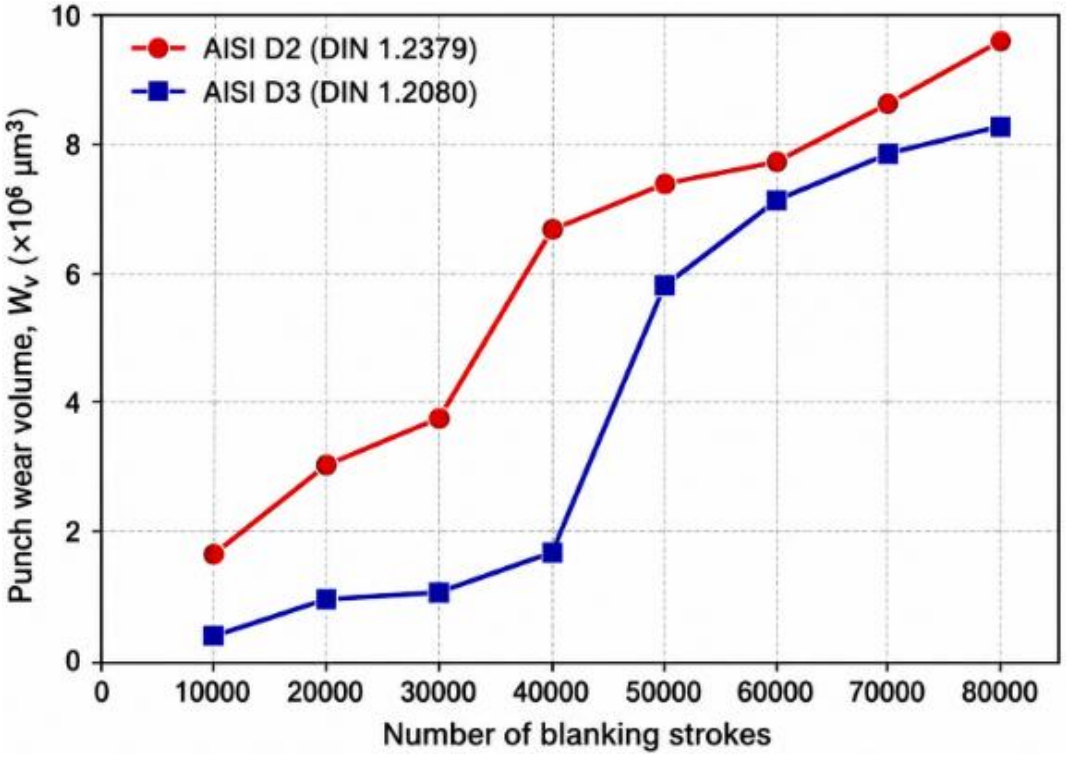


Fig. 10. Punch wear-volume evolution with number of blanking strokes for AISI D2 (DIN 1.2379) and AISI D3 (DIN 1.2080).

A notable feature of the dataset is the pronounced convergence of the D2 and D3 wear volumes beyond 50,000 strokes, illustrated directly in Fig. 11 through the D2/D3 wear-volume ratio, which falls from 4.77 at 10,000 strokes to just 1.17 at 80,000 strokes. This convergence is attributable to the onset of BUE formation on the D2 punch (Section 4.2): the transferred work piece material initially fills and partially masks the wear crater, which can transiently depress the net measured wear increment, before subsequent adhesive delamination of the built-up material accelerates the

apparent wear rate at later stages. The D3 punch, in maintaining a clean, purely abrasive wear mode throughout, exhibits a steadier and more predictable wear-volume trajectory a practically valuable property for maintenance-interval planning even where the absolute wear-volume gap with D2 has narrowed.

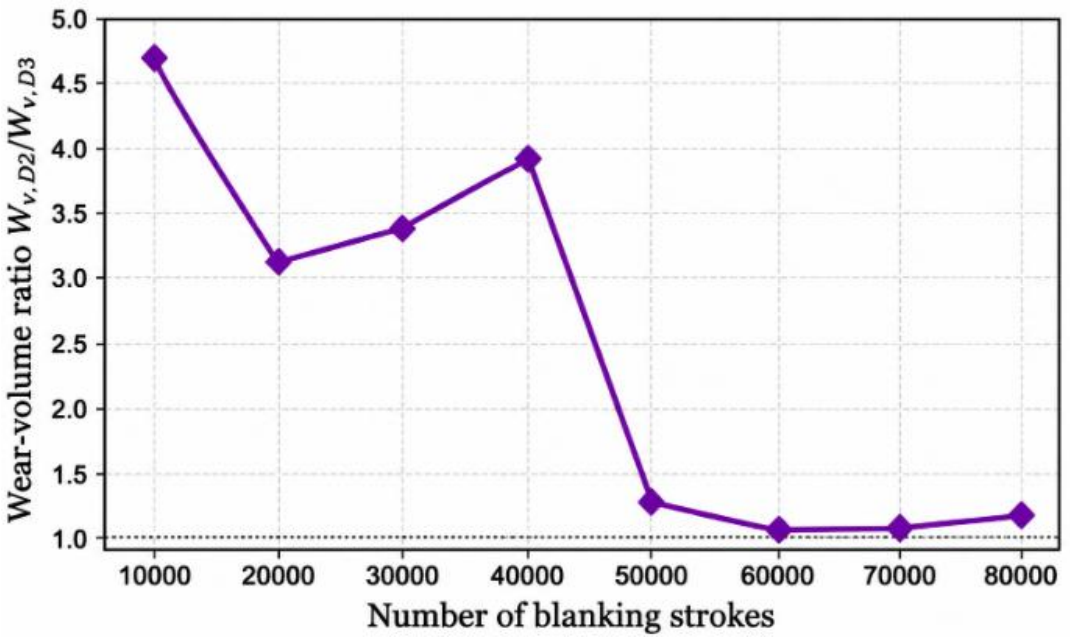


Fig. 11. Evolution of the AISI D2 / AISI D3 wear-volume ratio with number of blanking strokes, illustrating the pronounced convergence of wear performance beyond 50,000 strokes.

Independent probe-level measurements taken at multiple points around the punch perimeter (M1–M3) corroborate the trends identified above while also revealing the extent of local measurement variability (Fig. 12). The DIN 1.2080 (AISI D3) punch shows a steady, near-monotonic increase in linear wear from approximately 44 µm at 10,000 strokes to 127 µm at 80,000 strokes, with volumetric wear following a similarly gradual trend and peaking at approximately 8.2×10^6 µm³ behaviour that is highly predictable and well suited to scheduled maintenance planning. The DIN 1.2379 (AISI D2) punch, by contrast, shows an aggressive mid-cycle spike, with linear wear surging to nearly 159 µm at 50,000 strokes (approximately 35% higher than D3 at the same point) before both linear and volumetric wear plateau through 60,000–80,000 strokes; this non-monotonic behaviour is consistent with surface fatigue or micro-fracture accumulation around 50,000 strokes, followed by stabilisation associated with work-hardening or material transfer at the punch–work piece interface, and is in direct qualitative agreement with the BUE mechanism identified through microscopy. Probe-to-probe measurement spread is also evident: the D3 punch shows one

localised outlier at 60,000 strokes, while the D2 punch's probes remain tightly grouped through 50,000 strokes before diverging at 80,000 strokes, indicating the emergence of non-uniform wear around the cutting-edge perimeter at high stroke counts.

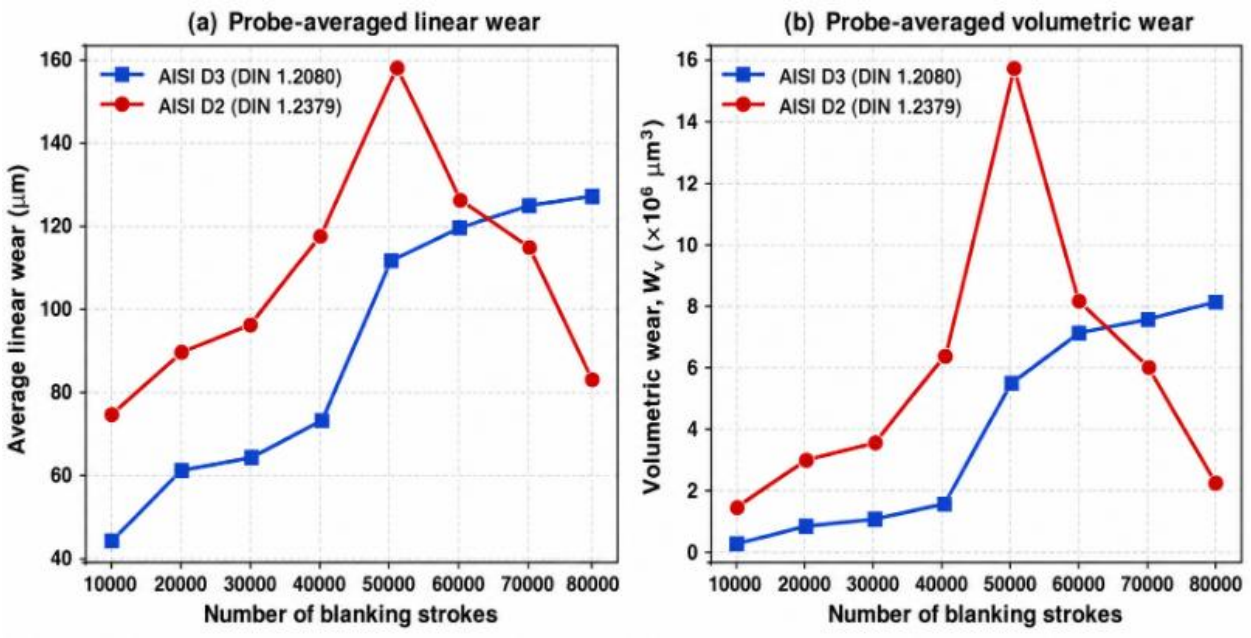


Fig. 12. Probe-level (M1–M3) linear-wear measurements around the punch perimeter for the DIN 1.2080 (AISI D3) and DIN 1.2379 (AISI D2) punches across the tested stroke range, illustrating both the mean wear trend and local measurement variability.

For completeness and to support independent re-analysis, the underlying average linear-wear values, volumetric-wear values, and probe-to-probe measurement spread (maximum − minimum across the M1–M3 probes) summarised in Fig. 12 are tabulated in Table 10.

Table 10. Supplementary probe-level linear-wear, volumetric-wear, and measurement-spread data for the DIN 1.2080 (AISI D3) and DIN 1.2379 (AISI D2) punches.

Strokes	D3 avg. linear wear (μm)	D2 avg. linear wear (μm)	D3 W_v (×10⁶ μm³)	D2 W_v (×10⁶ μm³)	D3 spread (μm)	D2 spread (μm)
10,000	45	75	0.3	1.5	19	25
20,000	62	90	0.9	3.0	16	22
30,000	65	97	1.1	3.6	25	44
40,000	75	118	1.6	6.5	21	18
50,000	112	158	5.6	15.8	58	11
60,000	120	126	7.2	8.1	83	10
70,000	125	115	7.6	6.0	13	12
80,000	127	83	8.1	2.3	52	20

The probe-level dataset in Table 10 corroborates the mean wear trends reported in Table 8 and Table 9 while additionally quantifying local variability: the pronounced spread increase for D3 (AISI D3 / DIN 1.2080) at 50,000–80,000 strokes (58–83 µm) indicates the emergence of non-uniform wear around the cutting-edge perimeter at high stroke counts, whereas the D2 (AISI D2 / DIN 1.2379) spread peaks earlier, near 30,000–40,000 strokes, before contracting once BUE-related material transfer partially homogenises the flank-wear profile.

4.4 Machine learning model performance

Table 11 summarises the performance of the three trained machine learning models on the held-out test set, and Fig. 13 presents the corresponding accuracy and error metrics graphically.

Table 11. Machine learning model performance on the held-out test set.

Model	R^2	RMSE (µm³)	MAE (µm³)	Training time
Random Forest	0.987	142,300	98,600	2.1 s
LSTM network	0.981	178,500	121,400	48 s
SVR (RBF)	0.962	256,800	189,200	0.4 s

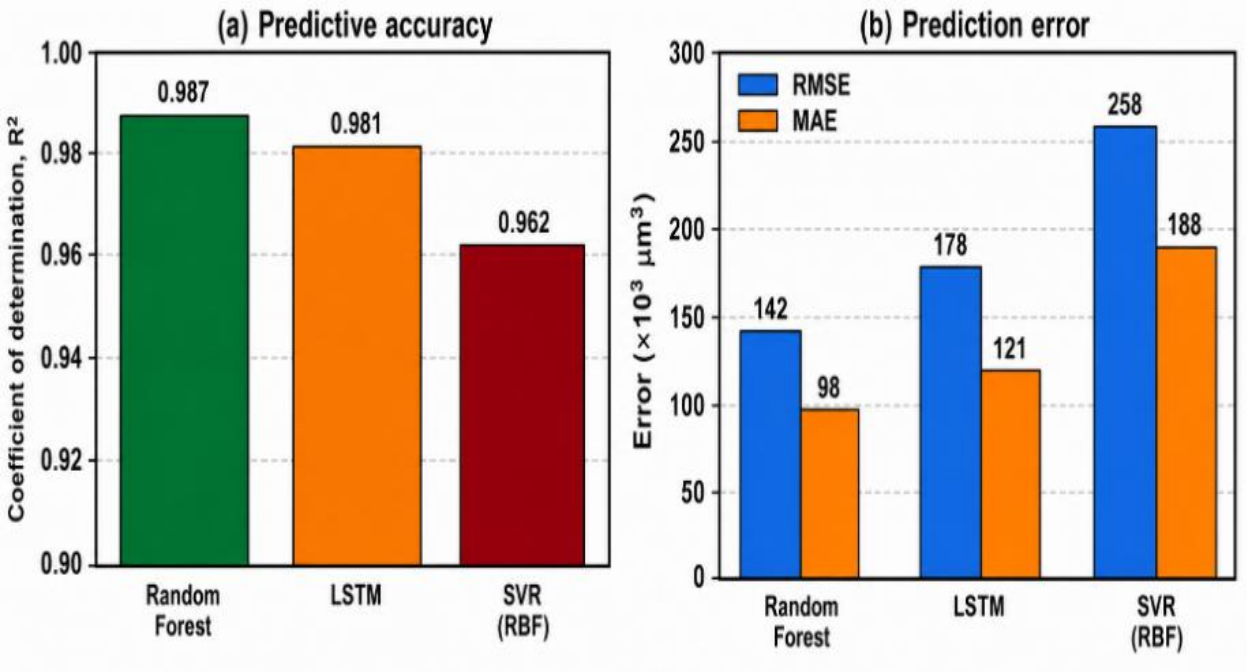


Fig. 13. Comparison of machine learning model performance on the test set: (a) coefficient of determination, R^2; (b) root-mean-squared error (RMSE) and mean absolute error (MAE).

The Random Forest model achieved the highest overall accuracy (R^2 = 0.987, RMSE = 142,300 µm³), closely followed by the LSTM network (R^2 = 0.981, RMSE = 178,500 µm³). Fig. 14 illustrates the agreement between actual and Random-Forest-predicted wear volumes across the test set, with data points for both materials clustering tightly around the ideal 1:1 fit line. The LSTM network's competitive performance, despite the modest size of the underlying experimental dataset, reflects its capacity to capture non-linear temporal dynamics in wear progression — in particular the inflection near 50,000 strokes associated with BUE formation on the D2 punch (Section 4.2) — at the cost of substantially longer training time (48 s versus 2.1 s for RF). The SVR model, while by far the fastest to train (0.4 s), under-performed relative to both the ensemble and deep-learning approaches (R^2 = 0.962, RMSE = 256,800 µm³), suggesting that the wear-volume prediction surface possesses sufficient non-linearity and local structure to benefit from non-parametric, tree- or sequence-based models over a fixed-kernel approach.

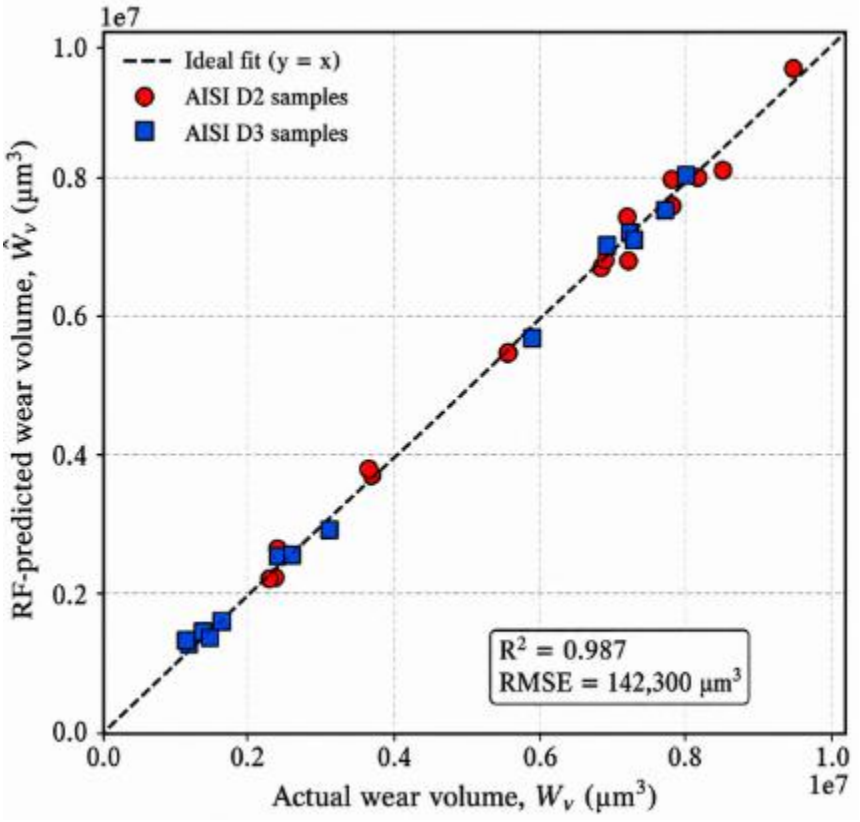


Fig. 14. Actual versus Random-Forest-predicted punch wear volume on the held-out test set for AISI D2 and AISI D3 samples, with the dashed line indicating the ideal 1:1 fit (R^2 = 0.987, RMSE = 142,300 µm³).

4.5 Feature importance analysis

Feature-importance analysis based on the mean decrease in impurity across the Random Forest ensemble is summarised in Table 12 and Fig. 15. Stroke count was identified as the dominant predictor of wear volume, accounting for 58% of total relative importance, followed by material hardness in HRC (22%), ultimate tensile strength (12%), and elastic modulus (8%). This ranking is physically consistent with the underlying wear mechanics: cumulative loading, represented by stroke count, is the primary driver of accumulated material loss, while hardness governs the punch material's intrinsic resistance to plastic deformation and abrasive material removal at the cutting edge. Tensile strength and elastic modulus, while secondary, contribute additional discriminating information related to the punch's resistance to micro-chipping and elastic deflection under repeated impact-shear loading.

Table 12. Random Forest feature-importance ranking for wear-volume prediction.

Rank	Feature	Relative importance (%)
1	Stroke count, N	58
2	Hardness, HRC	22
3	Tensile strength, R_m	12
4	Elastic modulus, E	8

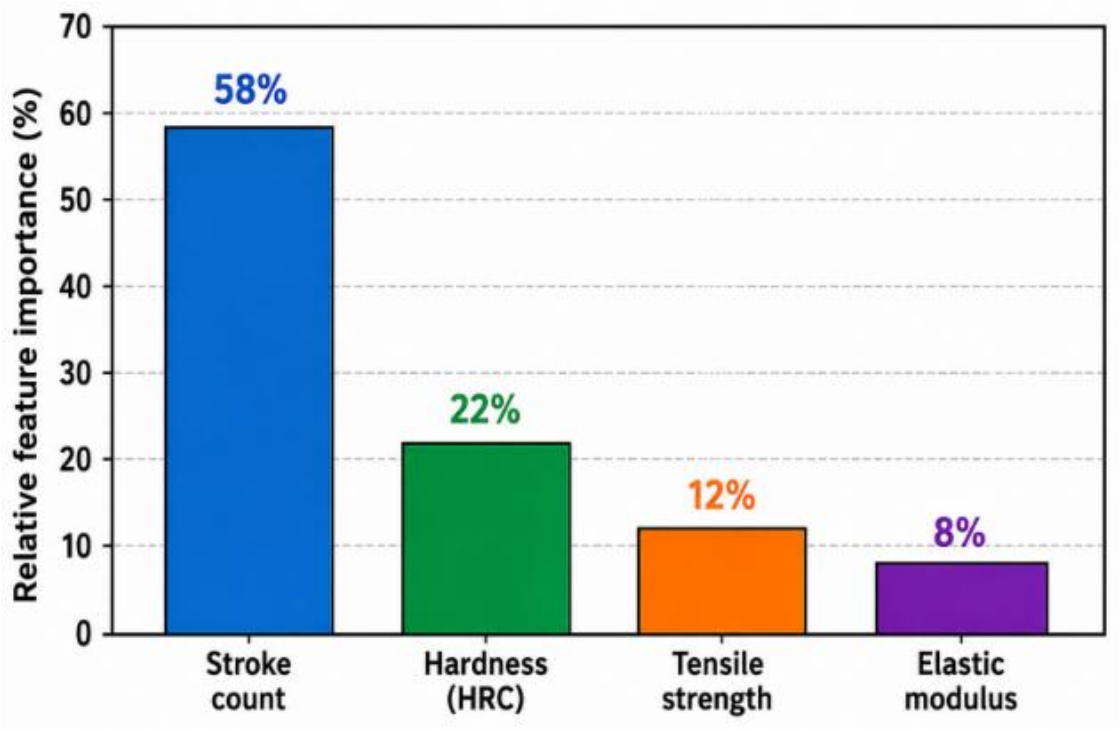


Fig. 15. Random Forest feature-importance ranking for prediction of punch wear volume, based on mean decrease in impurity (MDI).

4.6 Extrapolation behaviour and tool-life planning

An important practical consideration for deploying the trained models in tool-life planning is their behaviour when extrapolating beyond the 80,000-stroke upper bound of the training data. Because Random Forest predictions are constructed from piecewise-constant leaf-node averages, RF regressors are known to plateau rather than continue a learned trend when queried outside the range of the training data; consequently, RF-based wear-volume forecasts beyond 80,000 strokes should be treated as a conservative lower bound rather than a reliable point estimate. The LSTM model, being a continuous non-linear function approximator, is in principle better suited to smooth extrapolation, though its reliability beyond the observed stroke range remains unverified without additional experimental data at higher stroke counts. For near-term tool-change scheduling within the 10,000–80,000-stroke range explored experimentally, the RF model's high interpolative accuracy ($R^2 = 0.987$) makes it directly suitable for maintenance-interval planning; for longer-horizon forecasting, we recommend either extending the experimental stroke range or adopting a hybrid physics-informed approach in which the analytical wear model of Eq. (1) constrains the asymptotic behaviour of the data-driven predictor, as discussed further in Section 5.4.

5. Discussion

5.1 Mechanistic comparison of AISI D2 and AISI D3 wear behaviour

AISI D3 consistently outperforms AISI D2 across every measured wear metric. At 80,000 strokes, the D3 punch retains a cutting-edge radius approximately 40% lower than D2 (93.97 vs. 156.7 μm) and a wear volume approximately 14.5% lower (8.30×10^6 vs. 9.70×10^6 μm³). These differences can be traced to three material-level factors acting in combination. First, the higher carbon content of D3 (2.10 vs. 1.50 wt.%) promotes the formation of a greater volume fraction of chromium-carbide precipitates in the tempered martensitic matrix; these hard, discrete second-phase particles act as localised barriers to abrasive groove propagation and thereby raise the material's overall abrasive-wear resistance. Second, the higher bulk hardness of D3 (62 HRC vs. 59 HRC) directly reduces the susceptibility of the cutting edge to plastic deformation and edge rounding under the repeated impact-shear loading characteristic of blanking. Third, the absence of molybdenum in D3 avoids the formation of softer molybdenum-rich carbides that, in D2, can locally lower the effective wear resistance of the matrix under dry-contact sliding conditions.

The narrowing of the wear-volume gap beyond 50,000 strokes (Section 4.3) is a mechanistically and practically important finding. Mechanistically, it reflects a transition in the dominant wear regime on the D2 punch, from primarily abrasive material removal at low-to-moderate stroke counts to a combined abrasive-adhesive regime dominated by built-up-edge formation and subsequent delamination at higher stroke counts. Practically, it suggests that for very high-volume production runs (greater than approximately 50,000–60,000 parts per tool), the wear-volume advantage of D3 over D2 diminishes considerably, which may partially offset the higher material and machining cost typically associated with D3 tooling. Nevertheless, D3 continues to maintain a demonstrably cleaner cutting-edge profile, free of BUE-related surface irregularities, throughout the tested range — a quality-relevant advantage that persists even where the volumetric wear gap has narrowed. Tool-material selection for production runs exceeding approximately 60,000 strokes should therefore weigh burr-formation characteristics and cut-edge surface quality alongside volumetric wear rather than relying on wear volume as the sole selection criterion.

The present findings are broadly consistent with, and extend, prior tool-wear studies in blanking. Mucha [16] similarly reported that tool-material hardness and wear resistance strongly govern burr height evolution in generator-sheet blanking, while Akyürek et al. [25] found that both die clearance and punch hardness jointly determine tool-wear rate — a finding mirrored here by the strong RF-identified importance of hardness (22%) alongside stroke count. The magnitude of the wear-resistance advantage measured for D3 over D2 in the present dry-contact, high-stroke-count regime (up to 4.77× in wear volume at 10,000 strokes) is larger than typically reported for lubricated blanking trials in the literature, underscoring the particular importance of tool-material selection when lubrication is restricted or absent, as is often the case in food-contact, electronics, or coating-sensitive applications.

5.2 Comparative performance of the machine learning models

The superior performance of the Random Forest model relative to the LSTM and SVR models (Section 4.4) is consistent with several characteristics of the underlying dataset and problem structure. First, the experimental-plus-augmented dataset, while expanded to 150 records, remains modest by deep-learning standards; ensemble tree-based methods such as Random Forest are well known to be comparatively data-efficient and robust to small-sample regimes, since each tree is trained on a bootstrap resample and the ensemble average naturally regularises against overfitting

to any individual noisy observation. Second, the wear-volume-versus-stroke-count relationship exhibits a distinct piecewise structure — an approximately monotonic early-stage trend punctuated by the BUE-driven inflection near 50,000 strokes — that is naturally well captured by the axis-aligned, recursive-partitioning structure of decision trees, whereas the smooth, continuously differentiable function classes learned by SVR (with a fixed RBF kernel) and, to a lesser extent, LSTM networks may require more training data to resolve comparably sharp local transitions. Third, Random Forest offers a substantial practical advantage in interpretability: the feature-importance ranking (Section 4.5) provides direct, physically interpretable insight into the relative contribution of stroke count and material properties to wear evolution, a capability that is considerably more difficult to extract from a trained LSTM network without additional post-hoc interpretability techniques (e.g. SHAP or integrated gradients).

The LSTM network's close second-place performance ($R^2 = 0.981$) nonetheless demonstrates that sequence-aware deep-learning models can meaningfully capture non-linear, stroke-count-dependent wear dynamics even with a comparatively small training set, provided that appropriate regularisation (dropout) is applied. This capability may become increasingly valuable as future studies extend the feature set to include time-resolved process signals such as force–displacement curves or acoustic-emission signatures (Section 5.4), for which the LSTM architecture's ability to model temporal dependencies directly is a natural fit. The SVR model's comparatively lower accuracy, combined with its markedly lower training cost, positions it as a reasonable lightweight baseline for rapid screening applications where computational resources are constrained, but not as the preferred model for final tool-life prediction in the present application.

5.3 Industrial implications for tool-material selection

Taken together, the experimental and machine-learning findings support a stroke-count-dependent tool-material selection strategy. For production runs below approximately 50,000 strokes per tool change, AISI D3 offers a clear and quantifiable wear-resistance advantage, translating directly into extended maintenance intervals, reduced re-grinding frequency, and more consistent cut-edge quality. For production runs extending well beyond 60,000–80,000 strokes, the diminishing wear-volume advantage of D3 over D2 means that the higher unit cost of D3 tooling should be weighed against the narrower performance gap, while still accounting for D3's persistent advantage in burr-free, BUE-free cut-edge quality. The trained Random Forest model provides a practical, low-

computational-cost tool for supporting this decision: given a target production volume and candidate punch material properties, the model can generate a quantitative wear-volume forecast to inform maintenance-interval planning and material-cost trade-off analysis, without requiring a new, full-scale experimental wear campaign for every candidate tool-steel grade or heat treatment.

5.4 Toward hybrid, physics-informed, and sensor-integrated wear prediction

While the present data-driven models achieve strong interpolative accuracy within the tested stroke range, several avenues exist for strengthening their generalizability and industrial deployability. First, integrating the analytical wear-volume model of Eq. (1) directly into the machine learning framework for example, by using the analytical model as a physics-informed prior, regularisation term, or feature could improve extrapolation behaviour beyond the training range and reduce the data requirements for new tool-steel grades or process conditions. Second, augmenting the present feature set with additional process variables, including punch–die clearance, lubricant type or presence, and work piece thickness, would extend the model's applicability across a broader operating envelope and enable it to serve a wider range of blanking applications. Third, integration of online sensor data — particularly force–displacement signatures and acoustic-emission monitoring — with the trained models could enable real-time wear-state estimation and adaptive tool-replacement scheduling, moving beyond the current offline, interval-based measurement approach toward a genuine digital-twin capability for blanking tool management. Finally, cryogenic treatment of D2 and D3 punches represents a promising complementary wear-mitigation strategy, with literature reporting tool-life extensions of up to approximately two-fold for related cold-work tool steels [17,18]; incorporating cryogenic-treatment status as an additional categorical feature in future model iterations would allow the combined effect of material selection and heat-treatment strategy on wear evolution to be quantified within the same predictive framework.

5.5 Limitations

- The experimental dataset, while sufficient to reveal clear and mechanistically consistent trends, comprises only 15 original measurement records; the Gaussian-noise augmentation strategy (Section 3.2) mitigates but does not eliminate the risk of limited statistical power, and results should be corroborated with a larger, independently replicated dataset in future work.

- All tests were conducted at a single punch–die clearance (10% of sheet thickness) and a single work piece thickness (1 mm); the reported wear trends and model predictions should not be extrapolated to substantially different clearance ratios or sheet thicknesses without additional validation.
- Testing was restricted to dry-contact (unlubricated) conditions; lubricated blanking, which is common in many industrial settings, is expected to alter both the absolute wear rate and the relative balance between abrasive and adhesive wear mechanisms.
- As discussed in Section 4.6, the Random Forest model's tree-based structure limits its reliability when extrapolating wear-volume predictions beyond the 80,000-stroke upper bound of the training data; longer-horizon forecasts should be treated as indicative rather than definitive pending further experimental validation.
- The present study considers only two tool-steel grades (AISI D2 and D3); broader generalisation to other cold-work, high-speed, or powder-metallurgy tool steels would require additional experimental campaigns and corresponding model retraining.

6. Conclusions

This study combined a controlled experimental wear campaign with a data-driven machine learning framework to characterise and predict punch-wear evolution in blanking of ASTM A1011 sheet steel using AISI D2 and AISI D3 cold-work tool-steel punches. The following conclusions are drawn:

- AISI D3 exhibits superior wear resistance to AISI D2 across the full tested stroke range (10,000–80,000 strokes), attributable to its higher hardness (62 HRC vs. 59 HRC), greater tensile strength (1140 vs. 1052 MPa), and higher carbon content, which promotes chromium-carbide precipitation and enhances abrasive-wear resistance.
- AISI D2 punches experience combined adhesive and abrasive wear, with built-up-edge (BUE) formation evident beyond approximately 50,000 strokes, whereas AISI D3 punches undergo predominantly abrasive wear without material accumulation, maintaining a cleaner and sharper cutting edge throughout testing.

- Wear volume increases monotonically with stroke count for both materials, but the rate of increase is non-linear. The D2/D3 wear-volume ratio converges sharply from 4.77 at 10,000 strokes to 1.17 at 80,000 strokes, driven by BUE-related apparent wear suppression in D2 at intermediate stroke counts followed by accelerated adhesive delamination at higher stroke counts.
- The Random Forest model provides the most accurate wear-volume predictions (R^2 = 0.987, RMSE = 142,300 μm^3), outperforming both the LSTM neural network (R^2 = 0.981, RMSE = 178,500 μm^3) and the SVR model (R^2 = 0.962, RMSE = 256,800 μm^3); all three models nonetheless achieve practically useful accuracy for tool-life planning purposes.
- Random Forest feature-importance analysis identifies stroke count as the dominant wear predictor (58% relative importance), followed by hardness (22%), tensile strength (12%), and elastic modulus (8%), providing a physically interpretable ranking of the factors governing punch wear.
- For production runs below approximately 50,000 strokes, AISI D3 offers a clear wear-performance advantage; beyond approximately 60,000 strokes, the volumetric wear advantage narrows substantially, and supplementary criteria including burr formation and cut-edge surface-finish requirements should inform tool-material selection alongside volumetric wear alone.
- The combined experimental-and-machine-learning framework developed in this study offers a practical, computationally inexpensive route to predictive tool-life planning that can be extended to additional tool-steel grades, process parameters, and in-service sensor data without requiring a full mechanistic re-derivation for each new configuration.

Future work should extend the present feature set to include additional process variables punch die clearance, lubricant type, and work piece thickness to broaden the operating envelope over which the models remain valid, and should evaluate additional cold-work and powder-metallurgy tool-steel grades (e.g. Vanadis 4 and CPM 10V) under the same experimental protocol. Cryogenic treatment of both D2 and D3 punches represents a promising avenue for further wear-resistance enhancement, with literature reporting up to two-fold tool-life extension for related steels [17,18], and its incorporation as a categorical model feature would allow the combined effect of material selection and heat treatment to be quantified within a single predictive framework. Integration of

online sensor data (acoustic emission, force–displacement signatures) with the trained machine learning models would enable real-time wear-state monitoring and adaptive tool-replacement scheduling, while coupling finite-element modelling of the cutting-edge stress state with the present data-driven models could yield a hybrid, physics-informed machine learning framework for blanking-tool design and life prediction that combines the interpretability of mechanistic models with the flexibility and predictive accuracy of data-driven approaches.

Acknowledgement

The authors gratefully acknowledge the technical support provided by Kocaeli University and Anil Neerukonda Institute of Technology and sciences institutions in facilitating access to the blanking press, optical microscopy, and materials-testing facilities used in this study.

Author contributions

G.S.: conceptualisation, methodology, experimental investigation, writing original draft.

H.Ö.: materials characterisation, formal analysis, writing, review and editing.

N.K.K.: conceptualisation, methodology, machine learning modelling, data curation, writing original draft, review and editing. All authors have read and approved the final manuscript.

Funding

This research received no external funding.

Data availability

The datasets generated and analysed during the current study are available from the corresponding author upon reasonable request.

Conflicts of interest

The authors declare no conflicts of interest.

Nomenclature

Symbol / abbreviation	Description
t	Sheet thickness (mm)
D	Die opening diameter (mm)
d	Punch diameter (mm)
c	Punch–die clearance (mm)
F	Punch (blanking) force (N)
r	Punch cutting-edge radius (µm)
D_p	Punch diameter used in wear model (mm)
W_v	Wear volume (µm³)
N	Number of blanking strokes
R_m	Ultimate tensile strength (MPa)
E	Elastic modulus (GPa)
HRC	Rockwell hardness, C scale
R^2	Coefficient of determination
RMSE	Root-mean-squared error
MAE	Mean absolute error
AISI	American Iron and Steel Institute
ASTM	American Society for Testing and Materials
DIN	Deutsches Institut für Normung
BUE	Built-up edge
ML	Machine learning
RF	Random Forest
LSTM	Long short-term memory (neural network)
SVR	Support vector regression
MDI	Mean decrease in impurity
CV	Cross-validation

References

[1] Ma X, Kang Z, Pu C, et al. (2025). *Stamping part surface crack detection based on machine vision*. Measurement**,** 251, 117168. DOI: 10.1016/j.measurement.2025.117168

[2] Acar MC, Korkmaz HG, Toros S, Müller M (2025) Investigation and evaluation of formability of thin metallic bipolar plates by stamping process**.** *International Journal of Hydrogen Energy* **99**:203–211. DOI : 10.1016/j.ijhydene.2024.12.231

[3] Polajnar M, Čoga L, Sharma SK, Kalin M (2025) *Laboratory tribological screening test methodologies to evaluate the performance of metalworking lubricants for stamping. Tribology International* 211**:**110815.

[4] Gustafsson D, Parareda S, Ortiz-Membrado L, et al. (2023) *Simulation of metal punching and trimming using minimal experimental characterization. Journal of Materials Processing Technology* 321:118148.

[5] Lorenz M, Epple J, Donhauser C (2025) *Integrated measurement of tool wear in punching processes using a pneumatic gauging system. Wear* **570**:205928.

[6] Golovashchenko S, Zhou W, Nasheralahkami S, Wang N (2017) *Trimming and sheared edge stretchability of light weight sheet metal blanks. Procedia Engineering* 207:1552–1557.

[7] Li H, Wu X, Li G, Zhou D (2020) *Chipping damage of die for trimming advanced high-strength steel sheet. Journal of Materials Processing Technology* **285**:116787. DOI 10.1016/j.jmatprotec.2020.116787

[8] Zhou H, Li H, Zhao Y, et al. (2025) *Image-based AI-driven modelling for blank shape optimisation in sheet metal forming. Materials & Design* 256**:**114302.

[9] Lemiale V, Chambert J, Picart P (2009) *Description of numerical techniques for predicting the sheet metal blanking process by FEM simulation. Journal of Materials Processing Technology* 209:2723–2734. DOI 10.1016/j.jmatprotec.2008.06.021.

[10] Ikumapayi OM, Afolalu SA, Kayode JF, et al. (2022) *A concise overview of deep drawing in the metal forming operation. Materials Today: Proceedings* 62:3233–3238.DOI 10.1016/j.matpr.2022.03.530.

[11] Li S (2022) Sheet metal deep drawing for making metallic parts and structures**.** *Encyclopedia of Materials: Metals and Alloys*, pp. 182–196. DOI**:** 10.1016/B978-0-12-819726-4.00011-9

[12] Zhang X, Zhang H, Ren W (2018) Axial crushing of tubes fabricated by metal sheet bending**.** *Thin-Walled Structures* 122:252–263. DOI**:** 10.1016/j.tws.2017.09.023

[13] Muluneh DY, Johnson Santhosh A, Abate Lemma E, Murugan P (2022) Experimental investigation and process parameter optimization of sheet metal bending by line heating method**.** *Materials Today: Proceedings* 56(4):2398–2409. DOI: 10.1016/j.matpr.2021.12.45

[14] Basak S, Kim C, Jung YI, Jin HK, Lee MG (2022) Analyses of shearing mechanism during shear-cutting of 980 MPa dual-phase steel sheets using ductile fracture modelling and simulation**.** *International Journal of Material Forming* 15(1): Article 4. DOI: 10.1007/s12289-022-01654-y

[15] Pan M, Rao Y (2009) An integrated knowledge based system for sheet metal cutting–punching combination processing. *Knowledge-Based Systems* 22(5):368–375. DOI**:** 10.1016/j.knosys.2009.02.008

[16] Mucha J (2010) An experimental analysis of effects of various material tool's wear on burr during generator sheets blanking. *International Journal of Advanced Manufacturing Technology* **50**:495–507. DOI**:** 10.1007/s00170-009-2498-2

[17] Arslan Y, Uygur İ, Jazdzewska A (2015**)** The effect of cryogenic treatment on microstructure and mechanical response of AISI D3 tool steel punches**.** *Journal of Manufacturing Science and Engineering* 137(3):034501. DOI: 10.1115/1.4029801

[18] Arslan Y (2020) The effects of cryogenic process on the AISI M2 punch materials and on the hole edge geometry of the DIN EN 10111-98 sheet metal control arm parts**.** *Advances in Materials Science and Engineering* **2020**:Article ID 4685693. DOI: 10.1155/2020/4685693

[19] Arslan Y, Uygur İ, Bayraktar H (2013) An investigation of cryogenic treated cold work steel punch performance for AISI 304 stainless steel sheets**.** *Journal of Advanced Technology Sciences* **2**:61–75.

[20] Myint MH, Fuh JYH, Wong YS, Loh HT, Nee AYC (2003) Evaluation of wear mechanisms of Y-TZP and tungsten carbide punches**.** *Journal of Materials Processing Technology* 140(1–3):460–464. DOI: 10.1016/S0924-0136(03)00781-2.

[21] Luo SY (1999) Effect of the geometry and surface treatment of punching tools on tool life and wear in piercing of thick steel plate. J Mater Process Technol 88:122–133.

[22] Klocke F, Raedt H-W (2001) Formulation and testing of optimised coating properties in cold forging and fine blanking applications. Int J Refract Met Hard Mater 19:495–505. https://doi.org/10.1016/s0263-4368(01)00029-4

[23] Hambli R (2002) Design of experiment based analysis for sheet metal blanking processes optimisation. Int J Adv Manuf Technol 19:403–410. https://doi.org/10.1007/s001700200041

[24] Çavuşoğlu O (2022) An investigation of punch radius and clearance effects on the sheet metal blanking process. Int J Automot Sci Technol 6:309–316.

[25] Akyürek F, Yaman K, Tekiner Z (2017) An experimental work on tool wear affected by die clearance and punch hardness. Arab J Sci Eng 42:4683–4692.

[26] Jimbert P, Iturrondobeitia M, Ibarretxe J, Fernandez-Martinez R (2018) Influence of cryogenic treatment on wear resistance and microstructure of AISI A8 tool steel. Metals 8. https://doi.org/10.3390/met8121038

[27] Arslan Y, Seker U, Ozcatalbas Y, Ozdemir A (2016) An investigation of hole diameter and circularity on stainless steel sheets perforated via deep cryogenically treated cold work tool steel punches. J Eng Res Appl Sci 5:378–390..

[28] Hambli R (2003) BLANKSOFT: a code for sheet metal blanking processes optimization. J Mater Process Technol 141:234–242.

[29] Hambli R (2001) Blanking tool wear modeling using the finite element method. Int J Mach Tools Manuf 41:1815–1829.

[30] Hernández JJ, Franco P, Estrems M, Faura F (2006) Modelling and experimental analysis of the effects of tool wear on form errors in stainless steel blanking. J Mater Process Technol 180:143–150..

[31] Breiman L (2001) Random forests. Mach Learn 45:5–32

[32] Hochreiter S, Schmidhuber J (1997) Long short-term memory. Neural Comput 9:1735–1780
[33] Cortes C, Vapnik V (1995) Support-vector networks. Mach Learn 20:273–297..

[34] Wuest T, Weimer D, Irgens C, Thoben KD (2016) Machine learning in manufacturing: advantages, challenges, and applications. Prod Manuf Res 4:23–45.

[35] Bergs T, Holst C, Gupta P, Augspurger T (2021) Digital image processing with deep learning for automated cutting tool wear detection. Procedia Manuf 48:947–958.